# WRF-SOLAR

## Description and Clear-Sky Assessment of an Augmented NWP Model for Solar Power Prediction

BY PEDRO A. JIMENEZ, JOSHUA P. HACKER, JIMY DUDHIA, SUE ELLEN HAUPT, JOSE A. RUIZ-ARIAS, CHRIS A. GUEYMARD, GREGORY THOMPSON, TRUDE EIDHAMMER, AND AIJUN DENG

WRF-Solar is the first NWP model specifically designed to meet the growing demand for specialized numerical forecast products for solar power applications.

The variable nature of solar radiation at Earth's surface creates forecast challenges to maximize the exploitation of this renewable resource. For example, adequate planning reduces the cost of operation of power generating systems and allows for more efficient grid operations and confident bids in the energy market. An accurate solar power forecast is helpful to utilities that are managing the rapid increase in solar energy on the grid (e.g., Marquis et al. 2011). Burgeoning installed solar power capacity (Devabhaktuni et al. 2013) has greatly increased the demand for accurate forecasts.

The methodologies for solar power forecasting can be classified as one- or two-stage approaches (Chen et al. 2011). The first step in the two-stage approach consists of forecasting relevant meteorological variables such as the surface solar irradiance and, in the second step, transforming the meteorological forecasts into power production by modeling the solar conversion system. Different modeling approaches are available for the simulation of the photovoltaic (PV) systems (e.g., Zhou et al. 2007) or the concentrated solar thermal plants (CSP; e.g., Kraas et al. 2013). On the other hand, the one-stage approach does not model solar plant output and only uses available information to forecast the solar power production directly. The use of artificial intelligence in combination with historical data at the site is frequently used (e.g., Chen et al. 2011; Pedro and Coimbra 2012). The solar irradiance forecast is commonly used as an input to the one-stage approaches as well. Regardless of the approach selected, the challenge of solar power forecasting has been recognized to be essentially the same as for solar irradiance forecasting (Bacher et al. 2009).

Solar irradiance forecasts result from different methodologies depending on the temporal scales

**AFFILIATIONS:** JIMENEZ, HACKER, HAUPT, THOMPSON, AND EIDHAMMER—Research Applications Laboratory, NCAR, Boulder, Colorado; DUDHIA—Mesoscale and Microscale Meteorology Laboratory, NCAR, Boulder, Colorado; RUIZ-ARIAS—Solar Radiation and Atmosphere Modeling Group, Physics Department, University of Jaén, Jaén, Spain; GUEYMARD—Solar Consulting Services, Colebrook, New Hampshire; DENG—Department of Meteorology, The Pennsylvania State University, University Park, Pennsylvania
**CORRESPONDING AUTHOR:** Pedro A. Jimenez, Research Applications Laboratory, National Center for Atmospheric Research, 3450 Mitchell Ln., Boulder, CO 80301
E-mail: jimenez@ucar.edu

*The abstract for this article can be found in this issue, following the table of contents.*
DOI:10.1175/BAMS-D-14-00279.1

In final form 11 September 2015

(Diagne et al. 2013; Inman et al. 2013). Intrahour forecasts can follow from advection of clouds observed with ground-based all-sky cameras (e.g., Chow et al. 2011; Peng et al. 2015) or statistical methods based on other surface measurements (McCandless et al. 2015). Both linear and nonlinear statistical forecasting methods are also appropriate and widely used for intrahour forecasts (e.g., Reikard 2009; Mellit and Massi Pavan 2010). Analysis and extrapolation of satellite imagery shows good performance from ~30 min up to a maximum of 6 h (e.g., Hammer et al. 1999; Diagne et al. 2013; Nonnenmacher and Coimbra 2014). Because solar radiation is critically affected by small-scale dynamics and cloud microphysics (evaporation, condensation, etc.), the temporal autocorrelation of solar radiation time series can decrease rapidly. For prediction horizons beyond 6 h, numerical weather prediction (NWP) models become more appropriate and accurate (e.g., Perez et al. 2013). Some recent results suggest that forecasts from NWP models are also becoming competitive with statistical and satellite-based methods at shorter time scales (Diagne et al. 2013; Inman et al. 2013).

Despite the potential for NWP models to produce accurate shortwave forecasts across time scales, current NWP models often do not provide the most appropriate quantitative forecasts for the solar energy industry. Because weather predictions internally only require the global horizontal irradiance (GHI) for the model's energy budget, the direct normal irradiance (DNI) and diffuse (DIF) components are not commonly output to the user. GHI is much less sensitive to aerosol optical properties than DNI and DIF (e.g., Gueymard 2012; Ruiz-Arias et al. 2015), and sometimes NWP models do not account for atmospheric aerosols in the radiative transfer equation. This can be a limitation for CSPs, for example, which use the direct irradiance coming from the sun.

Aerosol modeling is often limited to models that explicitly consider atmospheric chemistry, whether run online (aerosols are explicitly modeled) with NWP or offline (aerosols properties are handled in a secondary application using NWP output). For example, the Weather Research and Forecasting (WRF; Skamarock et al. 2008) Model provides the WRF-Chem extension that accounts for atmospheric chemistry (Grell et al. 2005; Fast et al. 2006). Additional data to initialize the chemistry (e.g., sources of constituents) are required to solve chemistry equations and predict atmospheric aerosols. Chemical reaction equations and the advection of chemical species also considerably increase the computational cost and latency time. These technical limitations lead to limited use of explicit atmospheric chemistry in NWP for solar energy forecasts.

Aside from the aerosol direct effect (i.e., aerosol–radiation interactions), aerosols interact with cloud particles to modulate the cloud albedo and lifetime (Twomey 1974; Albrecht 1989). This is known as the aerosol indirect effect (e.g., Rap et al. 2013) and is usually only considered in NWP models that explicitly resolve atmospheric chemistry, if it is considered at all. Most models have independent cloud droplet radius and ice crystal size in the radiation and microphysics parameterizations (Stensrud 2007). The clouds are homogeneous in terms of the size of the microphysics species interacting with radiation, precluding the coupling required for the indirect effect. Improving these and other characteristics of NWP models is desirable to provide a better shortwave radiation forecasting framework that may foster the deployment of solar energy facilities.

**Table 1. Comparison of WRF and WRF-Solar developments.**

| | WRF-Solar | WRF |
|---|---|---|
| Solar energy applications | Output DNI and DIF | — |
| | High-frequency output of surface irradiance | — |
| | Solar position algorithm includes EOT | EOT is not included |
| Aerosol–radiation feedbacks | Observed/model climatologies or time-varying aerosols | Model climatology |
| Cloud–aerosol feedbacks | Aerosol indirect effect represented | — |
| Cloud–radiation feedbacks | Cloud particles consistent in radiation and microphysics | — |
| | Shallow cumulus feedback to radiation | — |
| | Fully coupled aerosol–cloud–radiation system | Uncoupled |

WRF-Solar was developed to fulfill specific needs of the solar energy industry, while avoiding the difficulty of complex aerosol modeling. The model builds on the WRF modeling framework and has been developed within a project funded by the Department of Energy (DOE) that seeks improvement in GHI and DNI forecasts across a range of scales by blending different forecasting methods into a unified forecast (Haupt 2013; see sidebar for additional information). Synergistic work funded by the Federal Aviation Administration (FAA) was also leveraged. WRF-Solar developments are being made available to the WRF community through the official WRF releases.

As a part of the DOE-funded project, WRF-Solar has been run quasi operationally over the contiguous United States (CONUS) since November 2014 and was run during the complete year of 2015. The model predicts the shortwave direct, diffuse, and global irradiances; local point forecasts are fed into a statistical postprocessing system called DICast (Mahoney et al. 2012) to be combined with several other NWP models to generate power predictions at stakeholder solar facilities (see sidebar). As of this writing, the solar power forecasting system already provides timely forecasts to commercial PV plants and distributed PV located in diverse environments such as the San Luis Valley in Colorado, the Central Valley of California, and Long Island, New York.

Here we describe the specific WRF-Solar developments (Table 1) and present results characterizing the model performance with an emphasis on surface solar irradiance during clear-sky conditions. Under clear skies, the aerosol direct effect is the largest source of uncertainty in the irradiance forecasts. This is especially the case for DNI. DNI is very sensitive to the aerosol load that can produce 100% of attenuation under certain conditions (Schroedter-Homscheidt et al. 2013). Since DNI is the

## SUNCAST: A COMPREHENSIVE SOLAR POWER FORECASTING SYSTEM.

WRF-Solar is an important component of the National Center for Atmospheric Research's (NCAR) SunCast Solar Power Forecasting System. This system seeks to compare the various methods of forecasting irradiance and to blend the different forecasts to provide a "best practices" comprehensive solar power forecasting system as displayed in the accompanying figure (Fig. SB1). In addition to WRF-Solar, irradiance forecasts from other high-resolution, regional, and global NWP models are blended and tuned via the Dynamic Integrated foreCast (DICast) system, producing a more accurate irradiance forecast on average than any component model for each lead time (Mahoney et al. 2012).

In addition, a suite of nowcasting models forecast in their sweet spots for the 0–6-h time range. TSICast, built by Brookhaven National Laboratory, utilizes data from multiple total-sky imagers (TSIs) to determine current cloud position, height, and depth and also the cloud movement at the different levels to project the position over the next 30 min (Peng et al. 2015). StatCast leverages local pyranometer measurements and trains regime-dependent artificial network models from 15 min out to 3 h (McCandless et al. 2015). In the 1–6-h time range, we include the satellite-derived cloud advection technique designed by scientists at the Cooperative Institute for Research in the Atmosphere at Colorado State University. (Rogers et al. 2015). NCAR also deploys a 9-km implementation of WRF-Solar for the 6-h time frame as well as the Multi-Sensor Advective Diffusive foreCast (MADCast) system, which assimilates infrared irradiances from multiple satellite instruments and advects those derived clouds with the dynamic core of WRF (Auligné 2014a,b). These nowcast systems are blended seamlessly with the Nowcast blender, which in turn is blended with the DICast output to produce irradiance forecasts. Both, the Nowcast blender and DICast take into account the recent skill of each forecast component in their consensus forecasts.

The irradiance forecasts are converted to power using an artificial intelligence method (regression model tree) trained to data specific to the site of interest. An analog ensemble method (Delle Monache et al. 2013; Alessandrini et al. 2015) is used to both further improve on the deterministic power forecast as well as to quantify the uncertainty. The final output is a probabilistic solar power forecast tuned to the specific site.

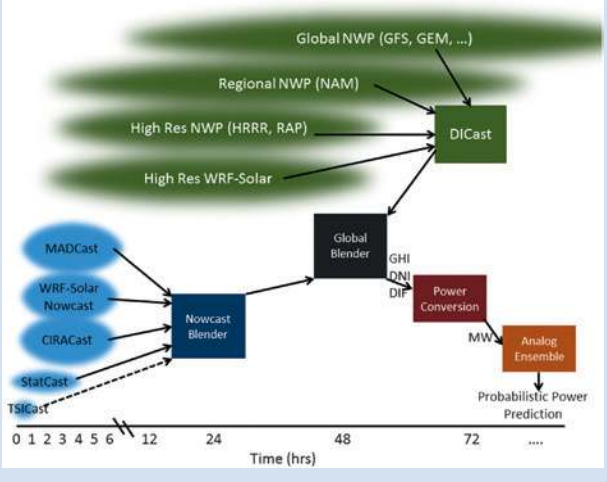


**Fig. SB1. Diagram of the SunCast Solar Power Forecasting System described in the sidebar.**

input to CSPs that mostly operate under clear skies, having an accurate DNI forecast under clear skies is essential for effective management. Hence, evaluating the clear-sky irradiance is a first solid step toward the solar power forecast under all-sky conditions.

Characterizing irradiance during partly cloudy to cloudy conditions will be the subject of a later contribution that will exploit the long-term simulations from the quasi-operational forecast intended to provide a statistically robust characterization of the cloud variability and its impact on the forecasts. Previous studies have validated that mesoscale models already have skill at predicting cloudiness (e.g., Guichard et al. 2003). Solar applications demand a more detailed validation of clouds (e.g., shallow cumulus) that remain subgrid scale at our target resolution and of the optical depths of resolved clouds. These validations are the primary areas for further development of the solar forecasting system. Cloud initialization is particularly crucial for short-range forecasts to inform both solar energy and convective storm forecasting.

**WRF-SOLAR DESCRIPTION.** WRF-Solar is a specific augmentation of the Advanced Research version of the WRF Model (Skamarock et al. 2008) designed to provide an improved NWP tool for solar energy applications. The WRF-Solar foundation is the official WRF version 3.6 released in 2014. We call the WRF lacking solar augmentation the "standard WRF" unless otherwise noted. In this section we document the WRF-Solar additions to the standard WRF. These include DNI and DIF available at temporal frequency limited only by model time step and several changes to model physics that account for feedbacks between aerosols, solar irradiance, and clouds. A conceptual diagram that illustrates these mechanisms is shown in Fig. 1.

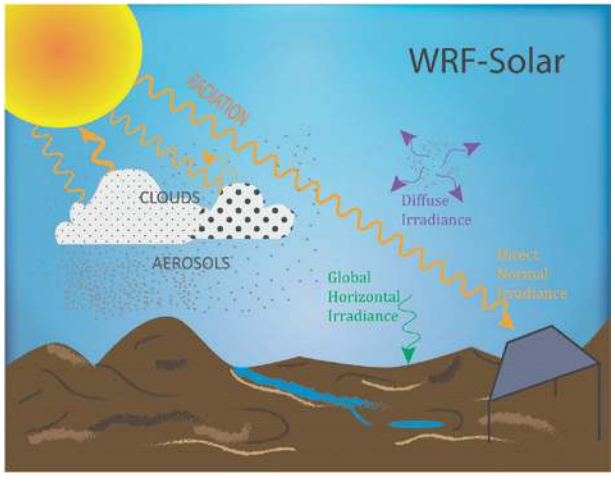


**Fig. 1. Sketch representing the physical processes that WRF-Solar improves. The different components of the radiation are indicated.**

Figure 1 also shows the different components of the irradiance. DNI is the irradiance received per unit of area over a surface perpendicular to the sun rays. DIF is the amount of surface irradiance that has been scattered by the atmosphere. GHI is the total amount of shortwave irradiance received by a surface horizontal to the ground and combines DIF and the component of DNI perpendicular to the ground.

*Physical additions for solar energy applications.* Many solar applications require direct and diffuse solar irradiance components in addition to GHI. For example, if the aim is to calculate the shortwave irradiance that impinges onto the plane of a solar panel, the typical computational method includes 1) projecting DNI onto the direction normal to the plane of the panel, 2) adding a fraction of DIF evaluated from a sky view factor (the fraction of the total-sky hemisphere that is visible from a point in the panel), and 3) adding a fraction of GHI resulting from surface reflectance onto the tilted plane of the panel. An additional application is CSP production for which DNI is the fuel responsible for the energy production (DIF cannot be concentrated). WRF-Solar addresses the need for separate direct and diffuse components by making them available in the WRF output and also in auxiliary output files at arbitrary time intervals as short as the time step length of the model.

At least two of the existing shortwave parameterizations in the WRF calculate the direct and diffuse radiative transfer equations [e.g., Goddard scheme and the Rapid Radiative Transfer Model for Global Circulation Models (RRTMG); Chou and Suarez (1999); Iacono et al. (2008)]. In these cases, WRF-Solar adds the surface irradiance components to the model output. Other shortwave schemes do not explicitly solve for the direct and diffuse components but provide GHI at the surface. Examples are the "Dudhia" scheme (Dudhia 1989) and an older Goddard scheme (Chou 1992). The advantage of these simpler parameterizations is that they are faster at solving the radiative transfer equation. For these parameterizations, the direct and diffuse components are estimated from GHI using a regression model trained on worldwide observations (Ruiz-Arias et al. 2010). The optical air mass and the clearness index modulate the regression from GHI to DIF.

Improvements in the solar position algorithm used in previous versions of WRF, particularly the equation of time (EOT; Müller 1995), are now included. Deviations associated with the eccentricity of Earth's

orbit and the obliquity of Earth previously caused irradiance leads and lags of up to 16 min, depending on the day of the year. The standard WRF, before version 3.5.1, neglects the EOT correction, which is normally inconsequential when running the radiation scheme approximately every half hour. Solar energy applications demand more frequent calls to the radiation scheme, and the leads/lags then introduce nonnegligible error. Simulations performed during a day close to a maximum lag reduced the root-mean-square error (RMSE) in GHI by 31%.

WRF-Solar aims to provide irradiance components at every time step while avoiding unphysical discontinuities. Typically the computational time of a model integration step calling the radiation parameterization is an order of magnitude longer than an integration step that skips it, and the radiative computations are done only about every 10 model steps at most. In between calls, the standard WRF assumes that irradiance is constant, introducing temporal discontinuities (steps) in irradiance values computed at the surface. Fast radiative transfer methods are sometimes included in NWP models to simulate irradiance every time step (e.g., Manners et al. 2009). In WRF-Solar, we have implemented a computationally efficient algorithm that interpolates the irradiance between successive calls to the radiation scheme considering only the change in the actual solar position and assuming the cloud extinction effect remains fixed to the latest computed value (a smart persistence approach).

One useful augmentation is irradiance output at time intervals limited only by the model time step. High-frequency time series of surface irradiance components are useful to model solar ramps (i.e., an abrupt change in the surface irradiance). Figure 2 illustrates a solar ramp event accurately predicted by WRF-Solar. The first part of the day features cloudy skies that block the DNI so that GHI equals the DIF. WRF-Solar predicts this with only a slight overestimation. Around 1700 UTC, scattered cloud conditions appear and clear-sky conditions alternate with clouds. WRF-Solar then simulates the different components of the irradiance but with less high-frequency variability because the modeled irradiance is more representative of a temporal (and spatial) average.

*Aerosol-radiation feedback: Aerosol direct effect.* Standard WRF simulations neglect the effects of atmospheric aerosols. The radiative impact of aerosols on GHI is relatively small, explaining the lack of attention to it for most meteorological applications. But it has been recognized that highly polluted conditions can lead to biases (Barbaro 2015).

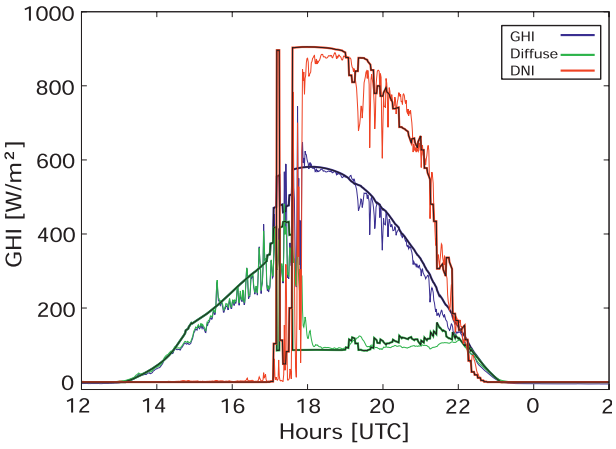


**Fig. 2. Observed and simulated surface irradiance components at site BND (see Fig. 5) during 2 Feb 2012. The simulation was initialized at 0000 UTC of the same day. The simulated irradiances are highlighted with a black solid line on top of the colored line that represents the irradiances (see legend).**

The standard WRF Model since version 3.5 has been capable of using a climatology-based aerosol parameterization developed at the European Centre for Medium-Range Weather Forecasts (ECMWF). The parameterization uses model results from Tegen et al. (1997) to derive monthly climatological means of the aerosol optical properties. Different models were used to simulate the transport of soil dust (Tegen and Fung 1995), sea salt, sulfate (Chin et al. 1996), and carbonaceous aerosols (Liousse et al. 1996). The 3D aerosol optical depth (AOD) for each species is on a grid with horizontal spacing of 5° longitude by 4° latitude and 12 pressure levels from 959 to 20 hPa. By activating the parameterization, which by default is turned off, the RRTMG shortwave parameterization infers the AOD from the combined effects of the species with their own assumed properties and uses them to solve for diffuse and direct irradiance. The AOD values remain constant, or change slowly, throughout the simulation period. This climatology and simple parameterization of aerosol effects are expected to allow a better representation of the direct and diffuse radiation components; no known previous attempts have been made to assess its performance before this work because the direct and diffuse irradiances were not previously available as output. Monthly mean aerosols are potentially useful but do not exploit current observations from satellites, surface networks, or from faster-evolving analysis/reanalysis products.

WRF-Solar allows the user to impose evolving aerosol optical properties in the simulation

(Ruiz-Arias et al. 2014), and considers humidity effects, to account for the aerosol direct effect. Parameterization of the effects of the aerosol optical properties on the radiation has been added to the Goddard (Chou and Suarez 1999; Shi et al. 2010) and the RRTMG (Iacono et al. 2008) shortwave radiation codes. The parameterization requires the total AOD at 0.550 $\mu$m (visible) and specification of the type of predominant aerosol. Knowledge of the predominant aerosol type allows for estimation of the remaining aerosol optical properties, including the single-scattering albedo and the asymmetry factor. It also permits modeling the spectral variability with estimations of the Ångström exponent. The user can optionally provide the single-scattering albedo, asymmetry factor, and Ångström exponent rather than allowing the parameterization to infer them based on the predominant aerosol. Ruiz-Arias et al. (2013) present a comparison of the parameterization to observations, which indicates that the parameterization produces accurate estimation of surface irradiance given accurate aerosol optical properties. Section 3 describes different aerosol datasets that are analyzed in the WRF-Solar model.

*Cloud–aerosol feedbacks*. Prior to version 3.6, the standard WRF lacked representation of aerosol interactions with cloud processes. To enable cloud–aerosol feedbacks and maintain computational affordability for operational applications, WRF-Solar borrows the simplified representation of the aerosol interaction with the Thompson microphysics (Thompson and Eidhammer 2014). Aerosol species are classified into hygroscopic and nonhygroscopic aerosols. The two species are currently initialized from a three-dimensional monthly climatology of the aerosol number concentrations generated from the Goddard Chemistry Aerosol Radiation and Transport (GOCART) model (Ginoux et al. 2001; Colarco et al. 2010). The surface emission flux is represented by a variable lower boundary condition based upon the starting aerosol conditions and an assumed mean surface wind.

As of the time of writing, the combination of the RRTMG radiation scheme and the Thompson and Eidhammer (2014) microphysics scheme fully incorporates the first and second aerosol indirect effects (Twomey 1974; Albrecht 1989). This adaptation of the standard WRF was aimed at NWP and WRF-Solar applications and resulted in minimal computational cost increase compared to running a full chemistry model [16% increase in simulation time compared to the previous Thompson et al. (2008) scheme]. Simulations of a large winter cyclone indicate the necessity of quantifying the benefits of the parameterization using long-term simulations to robustly quantify model forecast errors and observational uncertainty (Thompson and Eidhammer 2014).

*Cloud–radiation feedbacks*. Three further improvements in WRF close the aerosol–cloud–radiation feedback. First, consistency of the cloud particle distributions in the microphysics and radiation schemes is enforced. Historically, the cloud particle size for shortwave radiation calculations is imposed (i.e., the cloud effective radius is forced to remain constant) internal to a particular radiation scheme (Stensrud 2007). This implicitly assumes that all clouds are homogeneous in terms of their radii. To provide a more physically consistent representation of the cloud–radiation feedbacks, WRF-Solar adopts the novel approach of passing the effective radius of the cloud droplets, ice, and snow particles from the microphysics to the radiation (both shortwave and longwave) parameterization (Thompson and Eidhammer 2014; Thompson et al. 2015). This affects the cloud albedo and activates the aerosol indirect effects.

Second, the AOD from combined hygroscopic and nonhygroscopic aerosol number concentrations in the aerosol-aware microphysics can be passed to the radiation scheme. As noted above, the aerosols are currently initialized from a GOCART climatology. The aerosols are advected with the model dynamics. At a time step corresponding to a call to radiation physics, the extinction coefficient is computed and passed to the aerosol parameterization (Ruiz-Arias et al. 2014) for radiation. In this way, WRF-Solar provides a fully coupled representation of the aerosol–cloud–radiation system (Fig. 1).

The last development upgrades the feedbacks that subgrid-scale clouds produce in the shortwave irradiance. This effect is implemented in the shallow cumulus parameterization. The standard WRF Model does not typically provide a cloud fraction from its shallow subgrid convection parameterization options. WRF-Solar includes one shallow cumulus scheme previously implemented in the MM5 mesoscale model (Deng et al. 2003), which provides a cloud fraction for radiation. The Deng et al. (2003, 2014) shallow convection scheme is a mass-flux-based scheme. It includes a cloud entraining/detraining model to represent updrafts and it is triggered by factors including planetary boundary layer depth and turbulent kinetic energy (TKE). It uses a hybrid closure combining TKE and convective available potential energy, depending on the updraft depth.

In addition to the updraft formulation, the scheme also contains two predictive equations for cloud fraction and cloud liquid/ice water content for neutrally buoyant clouds (inactive clouds detrained from the active updraft core). Deng et al. (2014) shows that the scheme is able to produce reasonable cloud fractions and reduce surface temperature bias.

Initial testing of the parameterization at 9 km of horizontal resolution over CONUS shows a reduction of a positive bias in the GHI. The GHI bias at 14 sites distributed over the CONUS domain is shown in Fig. 3. The simulations were initialized at 1500 UTC and run for 6 h, spanning the complete year of 2014 with one simulation every week (52 simulations). Each simulation consists of a 10-member ensemble performed with the stochastic kinetic-energy backscatter scheme (SKEBS; Berner et al. 2011) implemented in WRF. Neglecting the effects of unresolved clouds introduces a systematic bias at the 14 sites (52 W $m^{-2}$). Activating the effects of the unresolved clouds reduces most of the bias (13 W $m^{-2}$, 75% of improvement). Several sites show a slightly negative bias, which indicates that the systematic overprediction of GHI is corrected.

The other shallow convection option used by WRF-Solar (Grell–Freitas) is also being adapted to provide a shallow cloud fraction to the radiation scheme.

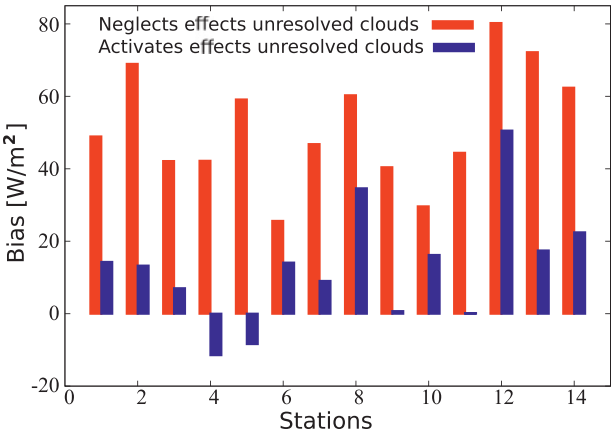


**Fig. 3. GHI bias at the seven sites from the SURFRAD network and the seven sites of the ISIS network with observations available for the year of 2014. The different lines represent simulations neglecting (red) and activating (blue) the effects of the unresolved clouds.**

**ASSESSMENT UNDER CLEAR-SKY CONDITIONS.** *Experiment details.* Six WRF-Solar experiments were completed to measure the importance of the aerosol direct effect on predictions of surface irradiance and to investigate sensitivity to aerosol optical property source and treatment. The first experiment (NO-AEROSOL) lacks any aerosol. The second experiment (ECMWF-CLIM) activates the ECMWF monthly climatology. The third experiment (SCS-CLIM) adds two further potential improvements: a monthly aerosol dataset covering North America at high spatial resolution (0.05° latitude by 0.05° longitude) developed by Solar Consulting Services (SCS) and a more sophisticated aerosol property parameterization for the aerosol direct effect. The fourth experiment (GOCART-CLIM) uses the GOCART climatology (section 2c) to activate the feedback to radiation (section 2d). GOCART-CLIM is the only experiment with aerosol advection and the only experiment where the Thompson microphysics aerosols are also used for the direct effect. SCS-CLIM and GOCART-CLIM impose the total AOD at 0.550 $\mu$m using data from models that explicitly predict evolving atmospheric chemistry. The fifth experiment (MACC-AOD) uses data from the ECMWF Monitoring Atmospheric Composition and Climate (MACC) reanalysis (Inness et al. 2013). MACC AOD is available globally every 3 h at 1.115° latitude by 1.115° longitude and here is linearly interpolated to hourly input to the WRF-Solar. The total AOD is a forecast variable starting from 0000 UTC analysis up to 24 h. The last (sixth) experiment (GEOS5-AOD) uses NASA's Goddard Earth Observing System model version 5 (GEOS5; Rienecker et al. 2000) analysis. The GEOS5 product is global and available every 3 h and is also interpolated to hourly AOD. The horizontal resolution is greater than the MACC at 0.5° latitude by 0.65° longitude. The experiments prescribing the AOD via the aerosol parameterization of WRF-Solar (i.e., SCS-CLIM, MACC-AOD, GEOS5-AOD) impose a rural-type (Shettle and Fenn 1979) predominant aerosol.

The high-resolution aerosol dataset for SCS-CLIM is composed of the AOD at 0.550 $\mu$m and the Ångström exponent for each month of the period 2000–14 and of the mean monthly single-scattering albedo. The methodology is similar to that used previously by other authors (Kinne et al. 2003, 2006; Kinne 2009; Kinne et al. 2013; Pappas et al. 2013) to develop climatologies including AeroCom, Hamburg (Pappas et al. 2013), and Max-Planck-Institute Aerosol Climatology (MAC; Kinne et al. 2013). They are composites based on remote sensing observations (spaceborne MODIS spectrometers and ground-based AERONET sunphotometers) and predictions from various aerosol transport models. Here, special attention was devoted to large parts of western North America where the Dark Target (DT) MODIS algorithm was found to considerably

overestimate AOD. Corrections to remove this bias over high-albedo areas (delineated from MODIS albedo data) were derived from a regional comparison with AERONET Level-2 data, Deep Blue MODIS data, MACC reanalysis, and the Hamburg climatology. The coarse spatial resolution (1° by 1°) of the original monthly gridded data were improved by combining a bilinear interpolation at sea level, and a correction to account for topographic effects on the vertical aerosol profile, using an exponential-scale height of 2.5 km. The Ångström exponent was obtained in a similar way, but without topographic correction. Among other differences with the MAC, the SCS dataset does not incorporate any specific AERONET data and does not force local agreement with ground truth.

Figure 4 compares the spatial variation of the AOD at 0.550 $\mu$m as obtained from monthly MODIS *Terra* (DT algorithm v5.1) and the SCS dataset at their respective spatial resolutions. This comparison is made for July in a climatological sense—that is, considering the long-term 2000–14 mean. In Fig. 4c, the time series of the monthly AOD obtained by AERONET (after appropriate spectral correction) is compared to the MODIS *Terra* and the SCS data for Maricopa, Arizona. Maricopa is one of the areas where the MODIS DT retrievals show a notable high bias. The SCS climatology reduces the high AOD bias providing a better comparison with the ground observations.

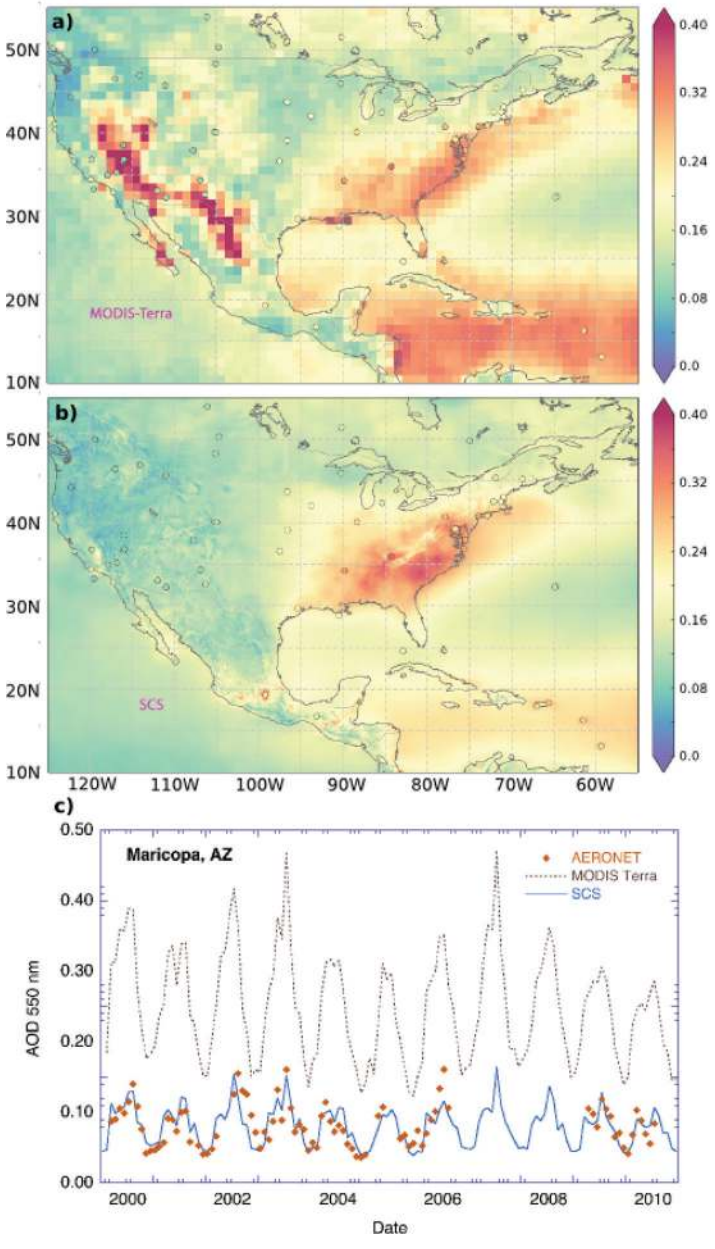


**Fig. 4. AOD at 0.550 $\mu$m from (a) MODIS and (b) the SCS dataset for the Jul climatology. (c) The time series at Maricopa, Arizona, are also shown together with the ground AOD observations. This figure demonstrates that the SCS dataset successfully removes the anomalous high bias in the western United States.**

WRF-Solar was configured similarly to NOAA's High-Resolution Rapid Refresh (HRRR) system, with the same physics schemes and on a domain covering the CONUS at 3-km horizontal grid spacing. One key difference from the HRRR is that our implementation calls the radiation code every 5 min compared to 30 min in the HRRR. Four periods of five consecutive days were selected for analysis in each season for a total of 20 days. All days were during 2012 because this is the most recent year with MACC reanalysis products available. Analyses from the Rapid-Refresh (RAP) model run by NCEP, with 13-km grid spacing, provided initial and boundary conditions every 3 h. Analyses were used to limit forecast error growth in this evaluation of aerosol direct-effect treatment. Initialization was at 0000 UTC each day, and simulations proceeded for 30 h to ensure a continuous daytime period in the simulations.

Verification is performed against irradiance observations from the Surface Radiation budget network (SURFRAD; Augustine et al. 2000, 2005). GHI, DNI, and DIF measurements are recorded every minute at seven geographically diverse sites across the CONUS (Fig. 5).

WRF-Solar was configured to output irradiance components at the SURFRAD sites every time step of the model (20 s), then these values were averaged to 1 min. With the present focus on clear-sky irradiance, the cloud–radiation feedback was deactivated. Verification samples were formed from all daytime minutes corresponding to clear skies in the observations, following Long and Ackerman (2000) to identify clear skies from observed GHI and DIF.

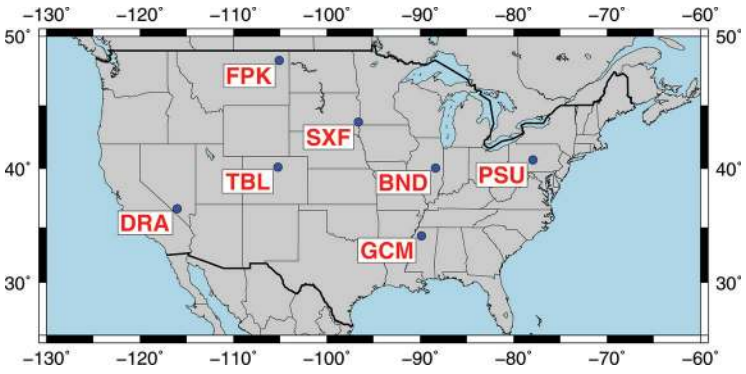


**Fig. 5. Location of the seven SURFRAD sites.**

*Results.* An example demonstrates the expected effects of aerosols on clear-sky irradiance. Aerosols absorb and scatter the incoming solar beam, reducing DNI and increasing DIF. Ignoring aerosols leads to systematic overprediction of DNI and underprediction of DIF. Figure 6a shows the observed irradiance during a nearly clear day at one SURFRAD site. Figure 6b shows the corresponding average errors (bias) for the NO-AEROSOL experiment. The simplest treatment for aerosols, ECMWF-CLIM, nearly eliminates bias in DIF and reduces the DNI bias magnitude (Fig. 6c). GHI is slightly overestimated, while DNI is slightly underestimated in the ECMWF-CLIM experiment. Bias in DIF is negligible. The impact on GHI is much weaker because absorption is small and scattering is highly peaked in the forward direction, but the GHI bias drops by more than 10 W $m^{-2}$. Bias in GHI should be the sum of the DNI and DIF biases but is not because of observational errors.

With few exceptions, the aerosol effect demonstrated in Fig. 6 generalizes to the full clear-sky dataset and other aerosol treatments (Figs. 7 and 8). The GEOS5 aerosols lead to the overall lowest bias magnitudes. Simulation at the GCM site is especially challenging for most of the experiments; GEOS5-AOD is the only experiment providing results comparable to those at the rest of SURFRAD sites. It will be shown below that this is a consequence of accurate AOD at GCM in the GEOS5. Although they improve on NO-AEROSOL, the SCS-CLIM, GOCART-CLIM, and MACC-AOD show too little DNI and too much DIF, thus indicating a high bias in the aerosol effect. A smaller magnitude impact on GHI is clear (Fig. 7c), but the relative improvement from the aerosol effect is large (Fig. 8c). Results from GEOS-5 suggest that computationally expensive models that explicitly and accurately solve the atmospheric chemistry can be competitive with, or superior to, high-quality climatology products.

RMSE improvements show that bias reductions from including aerosols are responsible for most of

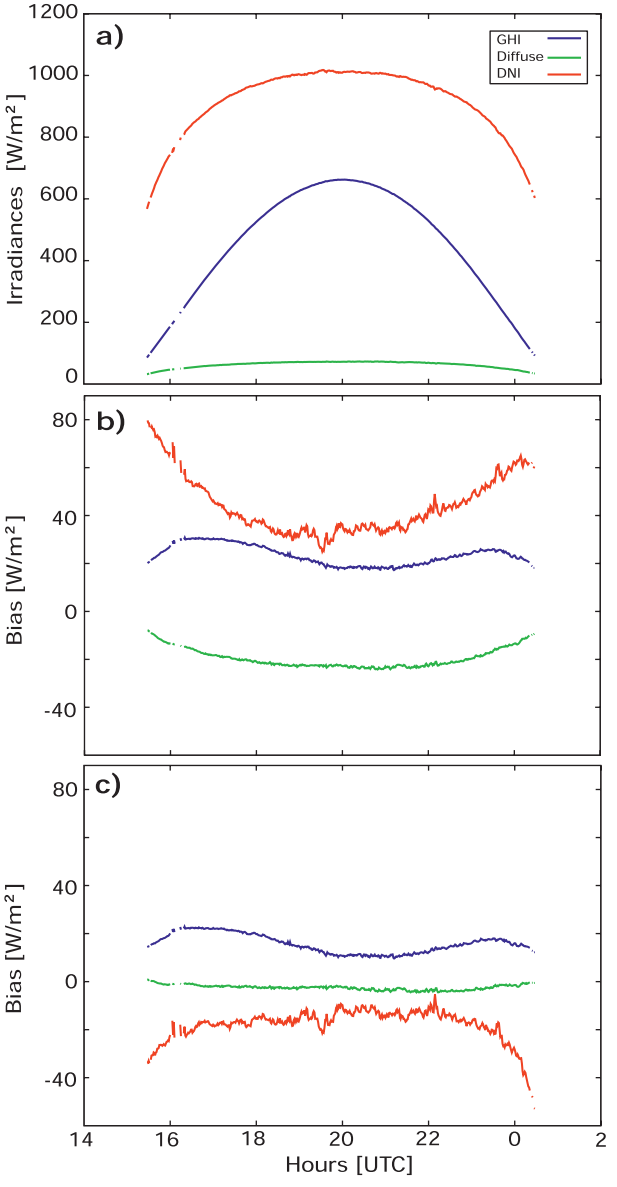


**Fig. 6. (a) Observed surface irradiance components and their biases from the (b) NO-AEROSOL and (c) ECMWF-CLIM experiments [see key in (a)] at site DRA during 4 Feb 2012.**

the error reductions (Table 2). Again, runs imposing climatological properties of the aerosol provide similar results, which are superior to the MACC-AOD and inferior to the GEOS5-AOD experiments. Almost all the experiments that include atmospheric aerosols reduce the RMSE compared to the NO-AEROSOL

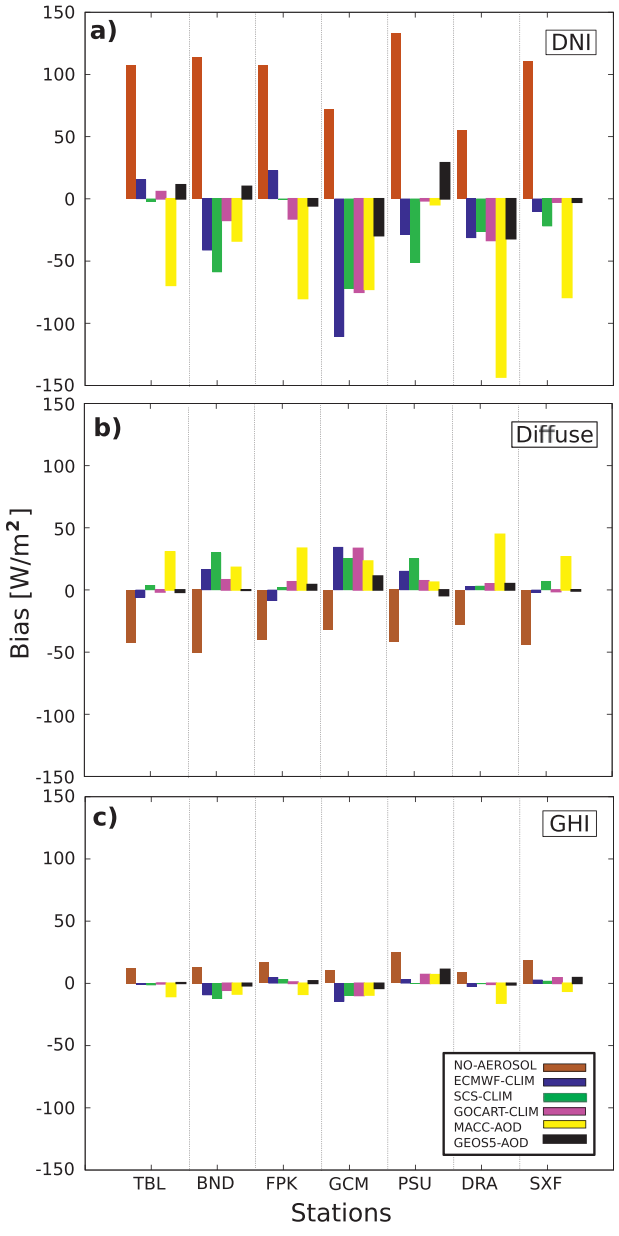


**Fig. 7. Biases in the surface irradiance components over all clear-sky minutes at each SURFRAD site. Results for the six numerical experiments are shown (see legend).**

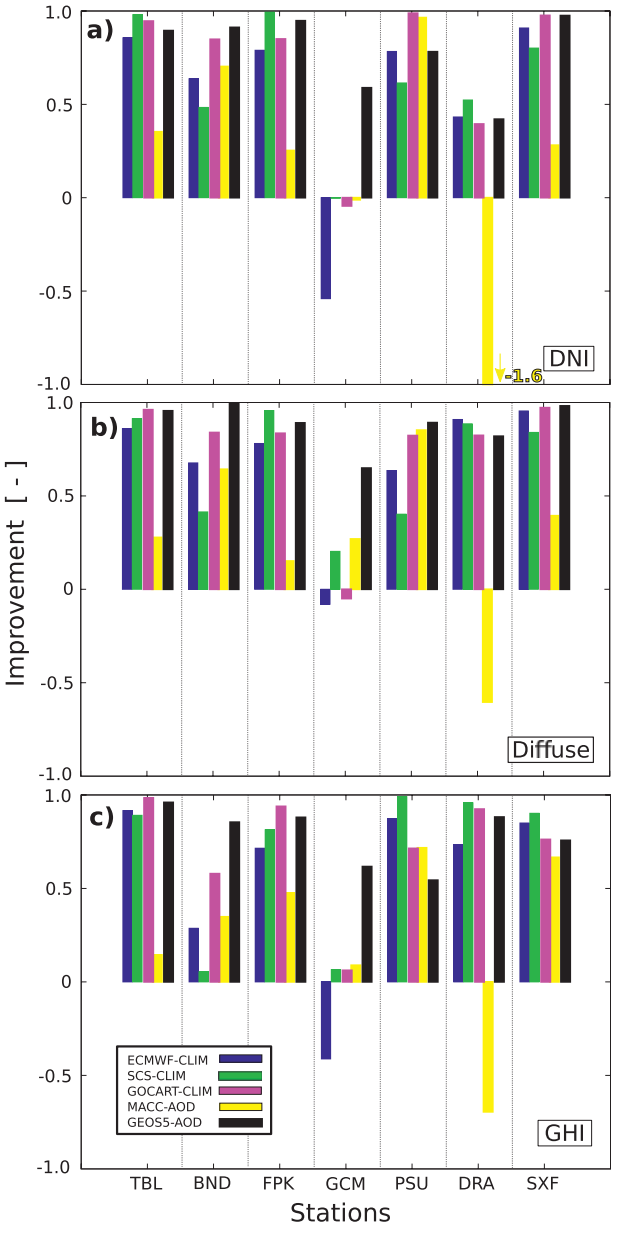


**Fig. 8. Improvements on the surface irradiance biases with respect to the NO-AEROSOL experiment for all clear-sky minutes.**

**Table 2. RMSE in the surface irradiance components (W m$^{-2}$). The relative improvement with respect to the NO-AEROSOL experiment is shown in parenthesis.**

| Irradiance | NO-AEROSOL | ECMWF-CLIM | SCS-CLIM | GOCART-CLIM | MACC-AOD | GEOS5-AOD |
|---|---|---|---|---|---|---|
| GHI | 21 | 16 (23%) | 16 (23%) | 16 (23%) | 20 (5%) | 15 (28%) |
| DIF | 44 | 20 (54%) | 19 (57%) | 26 (41%) | 42 (4%) | 12 (73%) |
| DNI | 103 | 66 (36%) | 52 (50%) | 58 (44%) | 120 (−16%) | 41 (60%) |

run, agreeing with the bias improvements (Figs. 7 and 8). The only exception is the RMSE of DNI for the MACC-AOD. Poor performance at DRA, where MACC strongly overestimates AOD (Figs. 7 and 8), is responsible. Again, the largest improvements are found using the GEOS5-AOD that shows improvements with respect to the ECMWF-CLIM, the standard representation of aerosols in NWP models, of 38% and 40% for the DNI and DIF, respectively.

Comparing temporal error variability from each experiment allows us to quantify the improvements associated with the AOD variability. Table 3 shows the standard deviation of the error defined as the differences between the simulation and the observations. Results from ECMWF-CLIM and GOCART-CLIM indicate that these experiments do not reduce the variability of the error, which indicates that the improvement in the errors (Table 2) is associated with a bias reduction. The variability of the error is higher in MACC-AOD than in the NO-AEROSOL experiment. On the contrary, SCS-CLIM and GEOS5-AOD reveal a reduction of the error variability. Experiment GEOS5-AOD shows the most error reduction compared to the standard approach, ECMWF-CLIM experiment, by 35% and 37% for the DNI and DIF, respectively.

The relative improvement of each model experiment is directly associated with accuracy in the aerosol optical properties. To verify this, the AOD recorded by the five multifilter radiometer channels available at the SURFRAD sites (0.4135, 0.4974, 0.6150, 0.6727, and 0.8698 $\mu$m) was interpolated to the primary wavelength of 0.550 $\mu$m using the observed Ångström exponent. The estimates from the five channels were then averaged to derive a single value. Comparing these observations to the values extracted from the four datasets under scrutiny here shows that the AOD skill among the various experiments is ranked similarly to the irradiance prediction skill (Fig. 9).

The SCS-CLIM aerosol reproduces noticeable characteristics in the observed AOD and agrees well with observations at certain sites (e.g., Fig. 9e). The

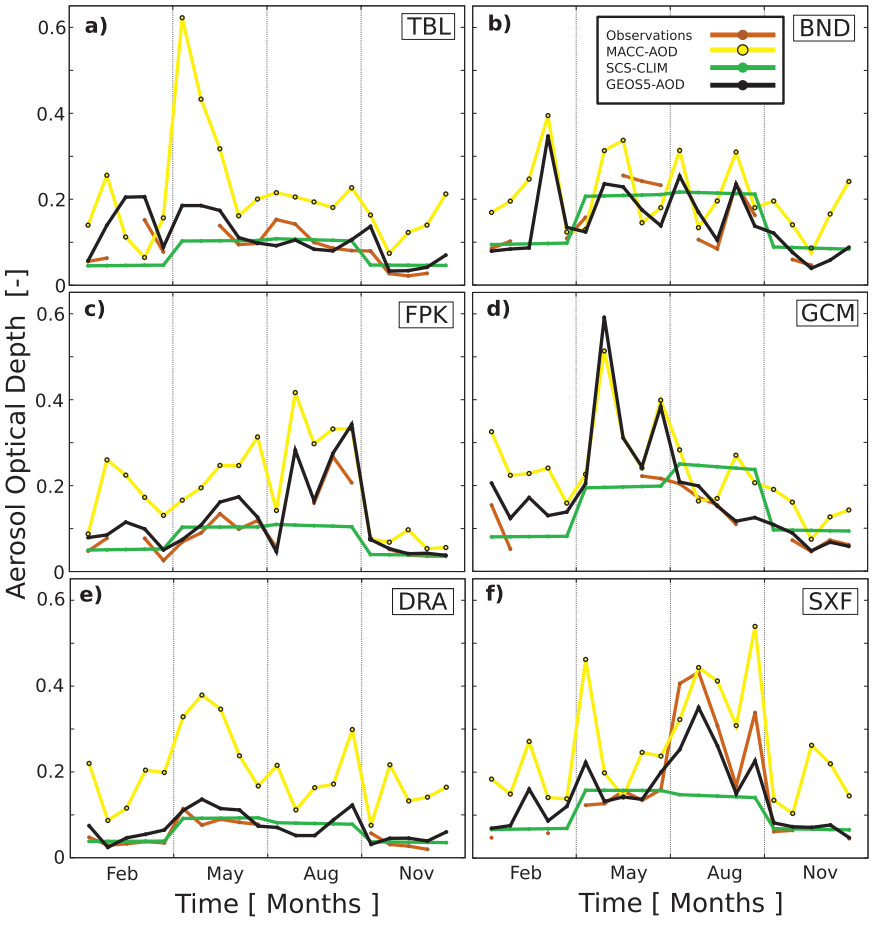


**Fig. 9. Total AOD at 0.550 $\mu$m from the different experiments at the SURFRAD locations with AOD records available.**

**Table 3. Standard deviation of the error in the surface irradiance components (W m$^{-2}$). The relative improvement with respect to the NO-AEROSOL experiment is shown in parenthesis.**

| Irradiance | NO-AEROSOL | ECMWF-CLIM | SCS-CLIM | GOCART-CLIM | MACC-AOD | GEOS5-AOD |
|---|---|---|---|---|---|---|
| GHI | 16 | 16 (0%) | 16 (0%) | 16 (0%) | 17 (−6%) | 15 (6%) |
| DIF | 23 | 19 (17%) | 17 (26%) | 25 (−9%) | 26 (−13%) | 12 (48%) |
| DNI | 52 | 62 (−14%) | 45 (13%) | 54 (−4%) | 77 (−16%) | 40 (23%) |

MACC-AOD and GEOS5-AOD both show temporal variability exceeding the observed AOD variability, with MACC-AOD additionally revealing a high bias. Site-specific AOD bias and correlation results (Table 4) clearly indicate that the GEOS5-AOD and SCS-CLIM both agree with observations better than MACC-AOD. This order is in agreement with the ability of the experiments to reproduce the observed surface irradiance (Fig. 8 and Table 2), indicating that RRTMG properly accounts for aerosol effects when supplied with appropriate inputs. This confirms other recent results (Gueymard and Ruiz-Arias 2015).

*WRF-Solar versus standard WRF.* To conclude the clear-sky assessment, a seventh numerical experiment summarizes the total effect of WRF-Solar (GEOS5-AOD) compared to the previous version of WRF that did not output separate irradiance components. The standard (baseline) WRF here is now defined as the official release of WRF version 3.5.1 with two modifications. First, the correction to the sun position algorithm was removed because it is part of the WRF-Solar effort. Second, code to output surface irradiance at the SURFRAD sites and at every model time step is added to enable direct comparison to WRF-Solar. WRF version 3.5.1 already included the WRF-Solar capability to output the direct and diffuse radiation components. Another difference with respect to the NO-AEROSOL experiment is that the standard WRF 3.5.1 does not include the interpolation of the modeled irradiance between radiation calls.

Figure 10 shows the decrease in RMSE in WRF-Solar simulations compared to those from the standard WRF. Consistent with earlier results, WRF-Solar improves the GHI, DNI, and DIF under clear-sky predictions at all SURFRAD sites. On average, GHI is improved by 46%, DNI by 60%, and DIF by 70%.

**Table 4. Bias/correlation of the total AOD at 0.550 $\mu$m at the SURFRAD sites (except PSU, which does not have AOD observations) for different experiments.**

| Station | SCS-CLIM | MACC-AOD | GEOS5-AOD |
|---|---|---|---|
| TBL | −0.01/0.59 | 0.09/0.38 | −0.01/0.72 |
| BND | 0.02/0.70 | 0.03/0.64 | 0.02/0.84 |
| FPK | −0.02/0.66 | 0.09/0.86 | −0.02/0.93 |
| GCM | 0.03/0.71 | 0.09/0.67 | 0.03/0.88 |
| DRA | 0.03/0.90 | 0.15/0.69 | 0.00/0.81 |
| SXF | −0.05/0.58 | 0.09/0.75 | −0.05/0.91 |

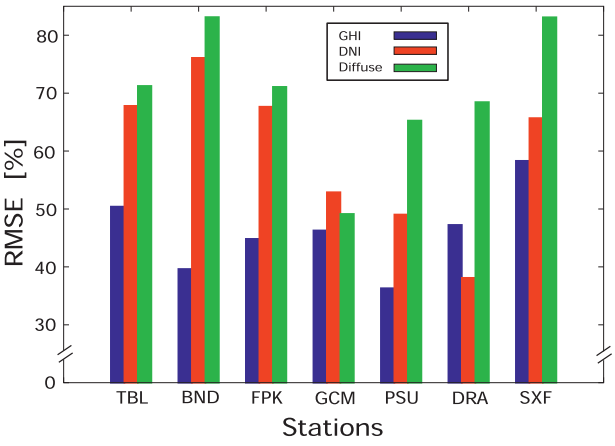


**Fig. 10. Improvements introduced by WRF-Solar (experiment GEOS5-AOD) in the estimations of the clear-sky surface irradiance components at the SURFRAD sites. The standard WRF simulation is used as a baseline for comparison.**

**CONCLUSIONS.** The WRF-Solar augmentations to the WRF Model, described here, result in the first NWP model specifically designed to meet the growing demand for specialized forecasting products associated with solar power applications. The model includes representation of aerosol–cloud–radiation feedbacks and efficient numerical approaches to support operational forecasting. This clear-sky assessment reveals large improvements compared to irradiance from the standard WRF. Sensitivity to details of the source of aerosol information emphasizes the importance of accurate aerosol optical properties for accurate estimates of surface irradiance. Models that explicitly solve atmospheric chemistry equations and are initialized with an aerosol data assimilation process (i.e., GEOS5) appear the most useful for clear-sky solar irradiance. In particular, imposing the temporal variability of the AOD produces large improvements in DNI and DIF with respect to the more extended use of aerosol climatologies.

Current developments focus on comparing forecasts and actual solar power production to precisely evaluate the model performance under all-sky conditions (including cloudy periods). Further modeling advances in WRF-Solar are expected from these efforts and should enhance the specific clear-sky improvements highlighted here. Included in these planned improvements are enhanced satellite data assimilation techniques. Combined with the ability to output high-frequency irradiance time series, the new WRF-Solar should prove helpful to the growing solar industry in general and contribute to better cloud, aerosol, and solar forecasts in general.

**ACKNOWLEDGMENTS.** This work was supported by DOE Project DE-EE0006016. The inclusion of cloud–aerosol feedbacks was conducted in response to requirements and funding by the Federal Aviation Administration. José A. Ruiz-Arias was funded by a Marie Curie Action under the Project PIOF-GA-2010-273648 within the Seventh European Community Framework Programme. The GEOS5 data used in this study was provided by the Global Modeling and Assimilation Office (GMAO) at NASA Goddard Space Flight Center. The authors thank the Monitoring Atmospheric Composition and Climate project funded under the European Union's Seventh Framework Programme for kindly providing the MACC AOD data.

## REFERENCES

Albrecht, B., 1989: Aerosols, cloud microphysics, and fractional cloudiness. *Science*, **245**, 1227–1230, doi:10.1126/science.245.4923.1227.

Alessandrini, S., L. Delle Monache, S. Sperati, and J. N. Nissen, 2015: A novel application of an analog ensemble for short-term wind power forecasting. *Renew. Ener.*, **76**, 768–781. doi:10.1016/j.renene.2014.11.061.

Augustine, J. A., J. J. DeLuisi, and C. N. Long, 2000: SURFRAD: A national surface radiation budget network for atmospheric research. *Bull. Amer. Meteor. Soc.*, **81**, 2341–2357, doi:10.1175/1520-0477(2000)081<2341:SANSRB>2.3.CO;2.

——, G. B. Hodges, C. R. Cornwall, J. J. Michalsky, and C. I. Medina, 2005: An update on SURFRAD—The GCOS surface radiation budget network for the continental United States. *J. Atmos. Oceanic Technol.*, **22**, 1460–1472, doi:10.1175/JTECH1806.1.

Auligné, T., 2014a: Multivariate minimum residual method for cloud retrieval. Part I: Theoretical aspects and simulated observations experiments. *Mon. Wea. Rev.*, **142**, 4383–4398, doi:10.1175/MWR-D-13-00172.1.

——, 2014b: Multivariate minimum residual method for cloud retrieval. Part II: Real observations experiments. *Mon. Wea. Rev.*, **142**, 4399–4415, doi:10.1175/MWR-D-13-00173.1.

Bacher, P., H. Madsen, and H. A. Nielsen, 2009: Online short-term solar power forecasting. *Sol. Energy*, **83**, 1772–1783, doi:10.1016/j.solener.2009.05.016.

Barbaro, E., 2015: Interactions between aerosol and convective boundary-layer dynamics over land. Ph.D. dissertation, Wageningen University, 182 pp.

Berner, J., S.-Y. Ha, J. P. Hacker, A. Fournier, and C. Snyder, 2011: Model uncertainty in a mesoscale ensemble prediction system: Stochastic versus multiphysics representations. *Mon. Wea. Rev.*, **139**, 1972–1995, doi:10.1175/2010MWR3595.1.

Chen, C., S. Ducan, T. Cai, and B. Liu, 2011: Online 24-h solar power forecasting based on weather type classification using artificial neural network. *Sol. Energy*, **85**, 2856–2870, doi:10.1016/j.solener.2011.08.027.

Chin, M., D. J. Jacob, G. M. Gardner, P. A. Spiro, M. Foreman-Fowler, and D. L. Savoie, 1996: A global three-dimensional model of tropospheric sulfate. *J. Geophys. Res.*, **101**, 18 667–18 690, doi:10.1029/96JD01221.

Chou, M.-D., 1992: A solar radiation model for use in climate studies. *J. Atmos. Sci.*, **49**, 762–772, doi:10.1175/1520-0469(1992)049<0762:ASRMFU>2.0.CO;2.

——, and M. J. Suarez, 1999: A solar radiation parameterization for atmospheric studies. NASA Tech. Rep. NASA/TM-1999-104606, Vol. 15, 38 pp.

Chow, C. W., B. Urquhart, M. Lave, A. Dominguez, J. Kleissl, J. Shields, and B. Washom, 2011: Intra-hour forecasting with a total sky imager at the UC San Diego solar energy testbed. *Sol. Energy*, **85**, 2881–2893, doi:10.1016/j.solener.2011.08.025.

Colarco, P., A. da Silva, M. Chin, and T. Diehl, 2010: Online simulations of global aerosol distributions in the NASA GEOS-4 model and comparisons to satellite and ground-based aerosol optical depth. *J. Geophys. Res.*, **115**, D14207, doi:10.1029/2009JD012820.

Delle Monache, L., F. A. Eckel, D. L. Rife, B. Nagarajan, and K. Searight, 2013: Probabilistic weather predictions with an analog ensemble. *Mon. Wea. Rev.*, **141**, 3489–3516, doi:10.1175/MWR-D-12-00281.1.

Deng, A., N. L. Seaman, and J. S. Kain, 2003: A shallow-convection parameterization for mesoscale models. Part I: Submodel description and preliminary applications. *J. Atmos. Sci.*, **60**, 34–56, doi:10.1175/1520-0469(2003)060<0034:ASCPFM>2.0.CO;2.

——, B. J. Gaudet, J. Dudhia, and K. Alapaty, 2014: Implementation and evaluation of a new shallow convection scheme in WRF. *26th Conf. on Weather Analysis and Forecasting/22nd Conf. on Numerical Weather Prediction*, Atlanta, GA, Amer. Meteor. Soc., 12.5. [Available online at https://ams.confex.com/ams/94Annual/webprogram/Paper236925.html.]

Devabhaktuni, V., M. Alam, S. Shekara Sreenadh Reddy Depuru, R. C. Green II, D. Nims, and C. Near, 2013: Solar energy: Trends and enabling technologies. *Renewable Sustainable Energy Rev.*, **19**, 555–564, doi:10.1016/j.rser.2012.11.024.

Diagne, M., M. David, P. Lauret, J. Boland, and N. Schmutz, 2013: Review of solar irradiance forecasting methods and a proposition for small-scale insular

grids. *Renewable Sustainable Energy Rev.*, **27**, 65–76, doi:10.1016/j.rser.2013.06.042.

Dudhia, J., 1989: Numerical study of convection observed during the Winter Monsoon Experiment using a mesoscale two-dimensional model. *J. Atmos. Sci.*, **46**, 3077–3107, doi:10.1175/1520-0469(1989)046<3077:NSOCOD>2.0.CO;2.

Fast, J. D., W. I. Gustafson Jr., R. C. Easter, R. A. Zaveri, J. C. Barnnard, E. G. Chapman, G. A. Grell, and S. E. Peckham, 2006: Evolution of ozone, particulates, and aerosol direct radiative forcing in the vicinity of Houston using a fully coupled meteorology-chemistry-aerosol model. *J. Geophys. Res.*, **111**, D21305, doi:10.1029/2005JD006721.

Ginoux, P., M. Chin, I. Tegen, J. M. Prospero, B. Holben, O. Dubovik, and S.-J. Lin, 2001: Sources and distributions of dust aerosols simulated with the GOCART model. *J. Geophys. Res.*, **106**, 20 255–20 273, doi:10.1029/2000JD000053.

Grell, G. A., S. E. Peckham, R. Schmitz, S. A. McKeen, G. Frost, W. C. Skamarock, and B. Eder, 2005: Fully coupled "online" chemistry within the WRF model. *Atmos. Environ.*, **39**, 6957–6975, doi:10.1016/j.atmosenv.2005.04.027.

Gueymard, C. A., 2012: Temporal variability in direct and global irradiance at various time scales as affected by aerosols. *Sol. Energy*, **86**, 3544–3553, doi:10.1016/j.solener.2012.01.013.

——, and J. Ruiz-Arias, 2015: Validation of direct normal irradiance predictions under arid conditions: A review of radiative models and their turbidity-dependent performance. *Renewable Sustainable Energy Rev.*, **45**, 379–396, doi:10.1016/j.rser.2015.01.065.

Guichard, F., D. B. Parsons, J. Dudhia, and J. F. Bresch, 2003: Evaluating mesoscale model predictions and parameterizations against SGP ARM data over a seasonal time scale. *Mon. Wea. Rev.*, **131**, 926–944, doi:10.1175/1520-0493(2003)131<0926:EMMPOC>2.0.CO;2.

Hammer, A., D. Heinemann, E. Lorenz, and B. Lückehe, 1999: Short-term forecasting of solar radiation: A statistical approach using satellite data. *Sol. Energy*, **67**, 139–150, doi:10.1016/S0038-092X(00)00038-4.

Haupt, S. E., 2013: A public-private-academic partnership to advance solar forecasting. *Proc. 42nd ASES Annual Conf.*, Baltimore, MD, American Solar Energy Society, 5 pp. [Available online at http://proceedings.ases.org/wp-content/uploads/2014/02/SOLAR2013_0284_final-paper.pdf.]

Iacono, M. J., J. S. Delamere, E. J. Mlawer, M. W. Shephard, S. A. Clough, and W. D. Collins, 2008: Radiative forcing by long-lived greenhouse gases: Calculations with the AER radiative transfer models. *J. Geophys. Res.*, **113**, D13103, doi:10.1029/2008JD009944.

Inman, R. H., H. T. C. Pedro, and C. F. M. Coimbra, 2013: Solar forecasting methods for renewable energy integration. *Prog. Energy Combust. Sci.*, **39**, 535–576, doi:10.1016/j.pecs.2013.06.002.

Inness, A., and Coauthors, 2013: The MACC reanalysis: An 8 yr data set of atmospheric composition. *Atmos. Chem. Phys.*, **13**, 4073–4109, doi:10.5194/acp-13-4073-2013.

Kinne, S., 2009: Climatologies of cloud-related aerosols. Part 1: Particle number and size. *Clouds in the Perturbed Climate System: Their relationship to Energy Balance, Atmospheric Dynamics, and Precipitation*, J. Heintzenberg and R. J. Charlson, Eds., MIT Press, 37–57.

——, and Coauthors, 2003: Monthly averages of aerosol properties: A global comparison among models, satellite data, and AERONET ground data. *J. Geophys. Res.*, **108**, 4634, doi:10.1029/2001JD001253.

——, and Coauthors, 2006: An AeroCom initial assessment—Optical properties in aerosol component modules of global models. *Atmos. Chem. Phys.*, **6**, 1815–1834, doi:10.5194/acp-6-1815-2006.

——, and Coauthors, 2013: MAC-v1: A new global aerosol climatology for climate studies. *J. Adv. Model. Earth Syst.*, **5**, 704–740, doi:10.1002/jame.20035.

Kraas, B., M. Schroedter-Homscheidt, and R. Madlener, 2013: Economic merits of a state-of-the-art concentrating solar power forecasting system for participation in the Spanish electricity market. *Sol. Energy*, **93**, 244–255, doi:10.1016/j.solener.2013.04.012.

Liousse, C., J. E. Penner, C. Chuang, J. J. Walton, H. Eddleman, and H. Cachier, 1996: A global three-dimensional model study of carbonaceous aerosols. *J. Geophys. Res.*, **101**, 19 411–19 432, doi:10.1029/95JD03426.

Long, C. N., and T. P. Ackerman, 2000: Identification of clear skies from broadband pyranometer measurements and calculation of downwelling shortwave cloud effects. *J. Geophys. Res.*, **105**, 15 609–15 626, doi:10.1029/2000JD900077.

Mahoney, W. P., and Coauthors, 2012: A wind power forecasting system to optimize grid integration. *IEEE Trans. Sustainable Energy*, **3**, 670–682, doi:10.1109/TSTE.2012.2201758.

Manners, J., J.-C. Thelen, J. Petch, P. Hill, and J. M. Edwards, 2009: Two fast radiative transfer methods to improve the temporal sampling of clouds in numerical weather prediction and climate models. *Quart. J. Roy. Meteor. Soc.*, **135**, 457–468, doi:10.1002/qj.385.

Marquis, M., J. Wilczack, M. Ahlstrom, J. Sharp, A. Stern, J. C. Smith, and S. Calvert, 2011: Forecasting

the wind to reach significant penetration levels of wind energy. *Bull. Amer. Meteor. Soc.*, **92**, 1159–1171, doi:10.1175/2011BAMS3033.1.

McCandless, T. C., S. E. Haupt, and G. S. Young, 2015: A model tree approach to forecasting solar irradiance variability. *Sol. Energy*, **120**, 514–524, doi:10.1016/j.solener.2015.07.020.

Mellit, A., and A. Massi Pavan, 2010: A 24-h forecast of solar irradiance using artificial neural network: Application for performance prediction of a grid-connected PV plant at Trieste, Italy. *Sol. Energy*, **84**, 807–821, doi:10.1016/j.solener.2010.02.006.

Müller, M., 1995: Equation of time—Problem in astronomy. *Acta Phys. Pol.*, **88A** (Suppl.), S49–S67.

Nonnenmacher, L., and C. F. M. Coimbra, 2014: Streamline-based method for intra-day solar forecasting through remote sensing. *Sol. Energy*, **108**, 447–459, doi:10.1016/j.solener.2014.07.026.

Pappas, V., N. Hatzianastassiou, C. Papadimas, C. Matsoukas, S. Kinne, and I. Vardavas, 2013: Evaluation of spatio-temporal variability of Hamburg Aerosol Climatology against aerosol datasets from MODIS and CALIOP. *Atmos. Chem. Phys.*, **13**, 8381–8399, doi:10.5194/acp-13-8381-2013.

Pedro, H. T. C., and C. F. M. Coimbra, 2012: Assessment of forecasting techniques for solar power production with no exogenous inputs. *Sol. Energy*, **86**, 2017–2028, doi:10.1016/j.solener.2012.04.004.

Peng, Z., D. Yu, D. Huang, J. Heiser, S. Yoo, and P. Kalb, 2015: 3D cloud detecting and tracking system for solar forecast using multiple sky imagers. *Sol. Energy*, **118**, 496–519, doi:10.1016/j.solener.2015.05.037.

Perez, R., and Coauthors, 2013: Comparison of numerical weather prediction solar irradiance forecasts in the US, Canada and Europe. *Sol. Energy*, **94**, 305–326, doi:10.1016/j.solener.2013.05.005.

Rap, A., C. E. Scott, D. V. Spracklen, N. Bellouin, P. M. Forster, K. S. Carslaw, A. Schmidt, and G. Mann, 2013: Natural aerosol direct and indirect radiative effects. *Geophys. Res. Lett.*, **40**, 3297–3301, doi:10.1002/grl.50441.

Reikard, G., 2009: Predicting solar radiation at high resolutions: A comparison of time series forecasts. *Sol. Energy*, **83**, 342–349, doi:10.1016/j.solener.2008.08.007.

Rienecker, M. M., and Coauthors, 2000: The GEOS-5 Data Assimilation System—Documentation of versions 5.0.1, 5.1.0, and 5.2.0. NASA Tech. Rep. NASA/TM-2008-104606, Vol. 27, 101 pp. [Available online at http://gmao.gsfc.nasa.gov/pubs/docs/GEOS5_104606-Vol27.pdf.]

Rogers, M. A., S. D. Miller, J. M. Haynes, A. Heidinger, S. E. Haupt, and M. Sengupta, 2015: Improvements in satellite-derived short-term insolation forecasting: Statistical comparisons, challenges for advection-based forecast, and new techniques. *13th Conf. on Artificial Intelligence*, Phoenix, AZ, Amer. Meteor. Soc., 6.4. [Available online at https://ams.confex.com/ams/95Annual/webprogram/Paper268850.html.]

Ruiz-Arias, J. A., H. Alsamanra, J. Tovar-Pescador, and D. Pozo-Vázquez, 2010: Proposal of a regressive model for the hourly diffuse solar radiation under all sky conditions. *Energy Convers. Manage.*, **51**, 881–893, doi:10.1016/j.enconman.2009.11.024.

——, J. Dudhia, F. J. Santos-Alamillos, and D. Pozo-Vázquez, 2013: Surface clear-sky shortwave radiative closure intercomparisons in the Weather Research and Forecasting model. *J. Geophys. Res. Atmos.*, **118**, 9901–9913, doi:10.1002/jgrd.50778.

——, ——, and C. A. Gueymard, 2014: A simple parameterization of the short-wave aerosol optical properties for surface direct and diffuse irradiances assessment in a numerical weather model. *Geosci. Model Dev.*, **7**, 1159–1174, doi:10.5194/gmd-7-1159-2014.

——, C. A. Gueymard, F. J. Santos-Alamillos, and D. Pozo-Vázquez, 2015: Do spaceborne aerosol observations limit the accuracy of modeled surface solar irradiance? *Geophys. Res. Lett.*, **42**, 605–612, doi:10.1002/2014GL062309.

Schroedter-Homscheidt, M., A. Oumbe, A. Benedetti, and J.-J. Morcrette, 2013: Aerosols for concentrating solar electricity production forecasts. *Bull. Amer. Meteor. Soc.*, **94**, 903–914, doi:10.1175/BAMS-D-11-00259.1.

Shettle, E., and R. W. Fenn, 1979: Models for the aerosols of the lower atmosphere and the effects of humidity variations on their optical properties. Air Force Geophysical Laboratory Tech. Rep. AFGL-TR-79-0214, 94 pp. [Available online at www.dtic.mil/cgi-bin/GetTRDoc?AD=ADA085951.]

Shi, J., and Coauthors, 2010: WRF simulations of the 20–22 January 2007 snow events over eastern Canada: Comparison with in situ and satellite observations. *J. Appl. Meteor. Climatol.*, **49**, 2246–2266, doi:10.1175/2010JAMC2282.1.

Skamarock, W. C., and Coauthors, 2008: A description of the Advanced Research WRF version 3. NCAR Tech. Note NCAR/TN-475+STR, 113 pp. [Available online at www.mmm.ucar.edu/wrf/users/docs/arw_v3_bw.pdf.]

Stensrud, D. J., 2007: *Parameterization Schemes: Keys to Understanding Numerical Weather Prediction Models.* Cambridge University Press, 478 pp.

Tegen, I., and I. Fung, 1995: Contribution to the atmospheric mineral aerosol load from land surface

modification. *J. Geophys. Res.*, **100**, 18707–18726, doi:10.1029/95JD02051.

——, P. Hollrig, M. Chin, I. Fung, D. Jacob, and J. Penner, 1997: Contribution of different aerosol species to the global aerosol extinction thickness: Estimates from model results. *J. Geophys. Res.*, **102**, 23895–23915, doi:10.1029/97JD01864.

Thompson, G., and T. Eidhammer, 2014: A study of aerosol impacts on clouds and precipitation development in a large winter cyclone. *J. Atmos. Sci.*, **71**, 3636–3658, doi:10.1175/JAS-D-13-0305.1.

——, P. R. Field, R. M. Rasmussen, and W. D. Hall, 2008: Explicit forecasts of winter precipitation using an improved bulk microphysics scheme. Part II: Implementation of a new snow parameterization. *Mon. Wea. Rev.*, **136**, 5095–5115, doi:10.1175/2008MWR2387.1.

——, M. Tewari, K. Ikeda, S. Tessendorf, C. Weeks, J. Otkin, and F. Kong, 2015: Explicitly-coupled cloud physics and radiation parameterizations and subsequent evaluation in WRF high-resolution convective forecasts. *Atmos. Res.*, **168**, 92–104, doi:10.1016/j.atmosres.2015.09.005.

Twomey, S., 1974: Pollution and the planetary albedo. *Atmos. Environ.*, **8**, 1251–1256, doi:10.1016/0004-6981(74)90004-3.

Zhou, W., H. Yang, and Z. Fang, 2007: A novel model for photovoltaic array performance prediction. *Appl. Energy*, **84**, 1187–1198, doi:10.1016/j.apenergy.2007.04.006.